# Procedings towards building an entangled photon pair source for novel applications in space.

Using ray-tracing analysis to provide a better understanding of the propagation, decoherence and coupling of down-converted photons.

**Adriaan Johannes Stolk**

Internship Report


*Supervisors:*
PI Dr. Alexander Ling
Dr. Kadir Durak
Centre for Quantum Technologies
National University of Singapore
13 02 2017

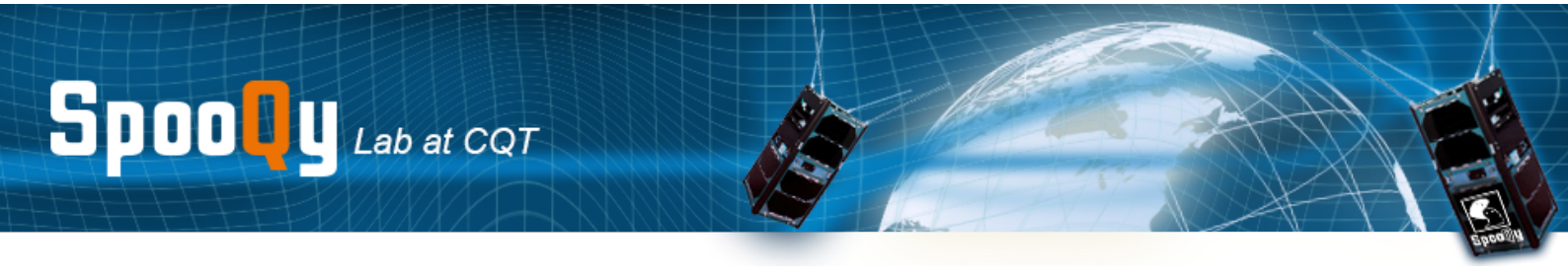

# Abstract

In this report, we study the properties of an polarization entangled two-photon state coming from our compact source, designed for space applications. The aim is to get a better understanding of the decoherence processes that occur in the generation of these entangled photons and to design methods that increase the brightness and entanglemet quality of the source. For this investigation a ray-tracing module in Mathematica is written, as well as professional ray-tracing software has been used.

The first result of this report is that one source of decoherence, the difference in arrival time between signal/idler pairs of the two polarizations, is dependant on the opening angle of the downconversion process. In our cross-crystal geometry leads to a collection of uncopmensated photons that decohere the state, reducing the fidelity with the maximally entangled Bell state. This problem can be solved by using different collection optics or using shorter crystals, as has been demonstrated by experiments and supported by simulations.

Secondly, to ensure stable and bright operation in a space environment, large line-width free running laser diodes would be preferred for pumping the source. Recent experiments have been unsuccessful in realizing a high fidelity entangled photon pair with these diodes. The reason for this observation has been recognized as the manufacturing tolerance on the crystal used in the source, a shortcoming of the used compensation method. The appropriate limits on the pump line-width and crystal machining have been identified, and a recommendation for ordering different components has been made. Other ideas to solve this have been proposed and are a topic of further research. We are confident that this will lead to a further improvement of the source.

These findings have shown the usefulness of the ray-tracing approach to this problem. Further recommendations on extending the model, as well as other aspects of the source that are already able to be tackled with the existing model, are recommended. This software will continue to perform a crucial role in the design and realization of a high performance, compact entangled photon source for novel applications in space.

# Contents

# Chapter 1

# Introduction

The generation of entangled photons using spontaneous parametric downconversion [1, 2, 3, 4] has been a topic of ongoing research for many decades now, both for theoretical and experimental physicists. Applications range from fundamental tests of nature[5, 6] and light-matter interactions [7], improved sensing techniques [8] and fundamentally secure communication through the use of quantum key distribution [9, 10] (QKD), sparking the interest of both academia and industry. Since the proposal of QKD using entanglement, many different approaches to generate a maximally entangled two photon state have been introduced [11, 12, 13], to be used in network schemes that can provide QKD over long distances. The lossy nature of communication with photons, and the absence of an efficient quantum repeater, limits the current range of any real-word implementation to $< 100$km.

To overcome this challenge, a space based solution using a fleet of small, cheap and robust cubesats is proposed by our research group [14, 15] . Among other technical challenges, this solution requires a high-visibility, compact and mechanically stable entangled photon source, which can survive the initial launch and harsh conditions in space. This source also has to comply with the size, weight and power (SWaP) restrictions when building a small satellite, heavily influencing the choices made in the design. In the past years the first steps in testing parts this source in space have been taken. The first iteration has proven to be able to survive a launch faillure [16] and proven successful in generating correlated photons on the Galassia mission [17].

This work will describe the current progress in the design of the compact entangled photon source and will introduce a custom written tool to simulate the performance of the source using a ray-tracing module written in Mathematica and OpticStudio 16.5. The initial results of this approach are presented, explaining some observations from experiment conducted in the group, that were previously not understood.

The lay-out of this report is as follows: in the next chapter some theoretical background of the SPDC process is given, necessary to understand the method used in our experiments. This also includes a theoretical description of the produced two photon state that in principle allows us to calculate the density matrix from the results of our simulations. Next the ray-tracing module in Mathematica is introduced, and some assumptions are justified. The chapter after that will show the results of simulating the performance of the entangled photon source and comparing it with experimental data. Next predictions will be made on the performance of the photon source when varying different parameters of our design. Finally a conclusion will be given to summarize what has been accomplished so far. Furthermore, the next steps in the design of photon source, as well as the possible improvements on the model and which aspects of the design to investigate next are discussed.

# Chapter 2

# Theory

This chapter will give the theoretical framework on which the findings of the next chapters are built. First a short description of the conditions under which spontaneous parametric down occurs is given, and the entangled photon source geometry used for this work is introduced. Next the spatial and temporal decoherence of this source is explained, and how to properly compensate them. Using a description the joint two photon amplitude of the state generated by this setup we can calculate the fidelity of the state produced by our entangled photon set-up with the desired Bell state. Finally the software used for the simulations is shortly introduced.

## 2.1 Theory

The generation of entangled photon pairs using the spontaneous parametric down-conversion (SPDC) is a phenomenon that, unlike other second-order effects, can not be described using the classical description of the electromagnetic field. It is best described quantum mechanically, where the interaction of a single pump photon of high energy and the vacuum state produce two photons of lower energy, historically called the signal and idler photon. The notion that the interaction is parametric means that it leaves the state of the material unperturbed. When we denote the angular frequencies of the pump, signal and idler light fields as $\omega_p$ , $\omega_s$ and $\omega_i$ respectively we can write down the energy conservation laws as follows:

$$\omega_p = \omega_s + \omega_i \tag{2.1}$$

To have have a sufficient interaction length of the three fields, the fields need to be phase-matched of a certain length $L$, which is usually but not always the crystal length. For large crystals and focused fields, the interaction length can be shorter than the crystal length. The phase matching condition can be written down as

$$\mathbf{k_p} = \mathbf{k_s} + \mathbf{k_i} \tag{2.2}$$

where $\mathbf{k_m}$, with frequency ($\omega_m$ $m = p, s, i$), is the three dimensional wave vector defined as

$$k_m = \|\mathbf{k_m}\| = \frac{\omega_m n_m}{c}.$$

Here, $c$ is the speed of light in vacuum and $n_m$ is the refractive index of the medium for the field $\omega_m$. This refractive index is usually not only a function of

frequency, but for some materials also of polarization, temperature of the medium and the direction of the light fields with respect to the optical axes of the medium.

It is a non trivial task to fulfill both Eq. 2.1 and 2.2 simultaneously. This task of phase-matching has been the topic of many years of research, and has led to a variety of different geometries, materials and tuning parameters used to build entangled photon sources, with varying degrees of success and complexity. We will only discuss the theory behind the approach that will be used in our experiments on the Spooqy missions.

## 2.2 Realizing phasematching

The method used to phase-match the interacting lightfields is called Type-I critical phasematching, where the birefringent properties of a uni-axial crystal of $\beta-BaB_2O_4$ ($BBO$) is used to result in a different refractive index for horizontally and vertically polarized light (with respect to the propagation direction). This property of birefrigence is a result of the specific crystalline structure of the material, and makes the refractive index a property of both polarization and propagation direction.

A uni-axial birefringent crystal can be described with one optical axis. Light that has its polarization lying on the plane that is *perpendicular* to this axis will experience an equivalent refractive index. This refractive index is called *ordinary* ($n_o$), and this refractive index will be constant no matter the propagation direction. For light that is polarized outside of this plane, the refractive index is a function of direction of propagation. This refractive index can vary between $n_o$ and the extraordinary refractive index ($n_e$). The ordinary and extraordinary refractive indices are called the principle indices of the medium, and are often determined using an empirical relation known as the Sellmeier formula:

$$n_{o,e}^2(\lambda) = A_{o,e} + \frac{B_{o,e}}{\lambda^2 - C_{o,e}} + E_{o,e}\lambda^2 \tag{2.3}$$

To calculate the refractive index for a photon that is extraordinary polarized for a given wave vector $\mathbf{k}$, the following formula can be used:

$$\frac{1}{n_{eff}^2} = \big(\frac{cos(\theta)}{n_o}\big)^2 + \big(\frac{sin(\theta)}{n_e}\big)^2 \tag{2.4}$$

where $\theta$ is the angle of the propagation direction with the optical axis. The birefringence of the crystals is defined as $\Delta n = n_e - n_o$, and a material is called positive (negative) birefringent when the birefringence is positive (negative). In all cases except for the extremes of $\theta = 0, \frac{\pi}{2}$, the extraordinary polarized ray experiences an effect called walk-off. This is a spatial shift of the extraordinary ray from the ordinary propagation direction. This is due to the fact that the Poynting vector is no longer in the same direction of the wave vector. This is an effect that is known to limit the interaction length of the SPDC process in birefringent crystals for certain configurations. The walk-off can be calculated using the formula

$$\rho = \frac{L}{2} n_{eff}(\theta)^2 * \big((\frac{1}{n_o})^2 - (\frac{1}{n_e})^2\big) * \sin(2\theta), \tag{2.5}$$

where $\theta$ is the angle with the optical axis, $L$ the interaction length and the refractive indices as defined in 2.4 We can now design the propagation through the crystal such

that we can satisfy both Eq. 2.1 and 2.2 simultaneously. This is done by cutting the face of the crystal such that the optical axis is at an angle with the propagation direction. Because BBO is a negative birefringent crystal and due to the dispersion of the fields and the energy conservation, the pump photon needs to be extraordinary polarized. Depending on the desired signal and idler wavelengths and propagation direction, one or both of the downconverted photons will be ordinary polarized. The type of phasematching where the signal and idler are co-polarized is called Type-I, and Type-II when the have different polarization.

Moreover, we can also make sure that the signal and idler photons propagate with an angle with respect to the incoming pump photon. This opening angle will be the direction for which the phasematching condition will be satisfied, and where the emission is possible. This angle can be zero, for which we call the geometry collinear, or small but non-zero, for which the geometry is called non-collinear.

All these properties of the downconversion process need to be taken into account when designing an entangled photon source, and are usually difficult to change once the specific BBO crystals are cut and ordered. That is why it is called critical phase matching, where the cut angle of the crystal will define the behaviour of the downconversion in the source.

## 2.3 Setup configuration

For our experiments we use a cross-crystal geometry of two BBO crystals phase-matched using Type-I phasematching to produce a signal ($\lambda \approx 785$nm) and idler ($\lambda \approx 832$nm) pair when pumped with a $\lambda = 405$nm blue laser diode. The pump is a single Gaussian mode, focussed using an aspheric lens into the crystals. The crystal cut that has to be used for these wavelengths is $\theta_c = 28.7991°$. The optical axis of the second crystal is rotated 90 degrees with respect to the first crystal. The pump beam is polarized 45 degrees, between the optical axes of the crystals. The crystals produce a correlated photon pair, where the downconverted photons are either both horizontally or both vertically polarized, depending on which crystal the pump photon got downconverted. After filtering out the pump beam, two more BBO crystal with the same crystal cut are added, half the length of the previous two. This is to spatially compensate the photons, more on that in the upcoming section. The photons are then collected into a single mode fibre, using focussing optics. The exact configuration of these lenses is still a work in progress. A schematic of the setup is shown in fig. 2.1.

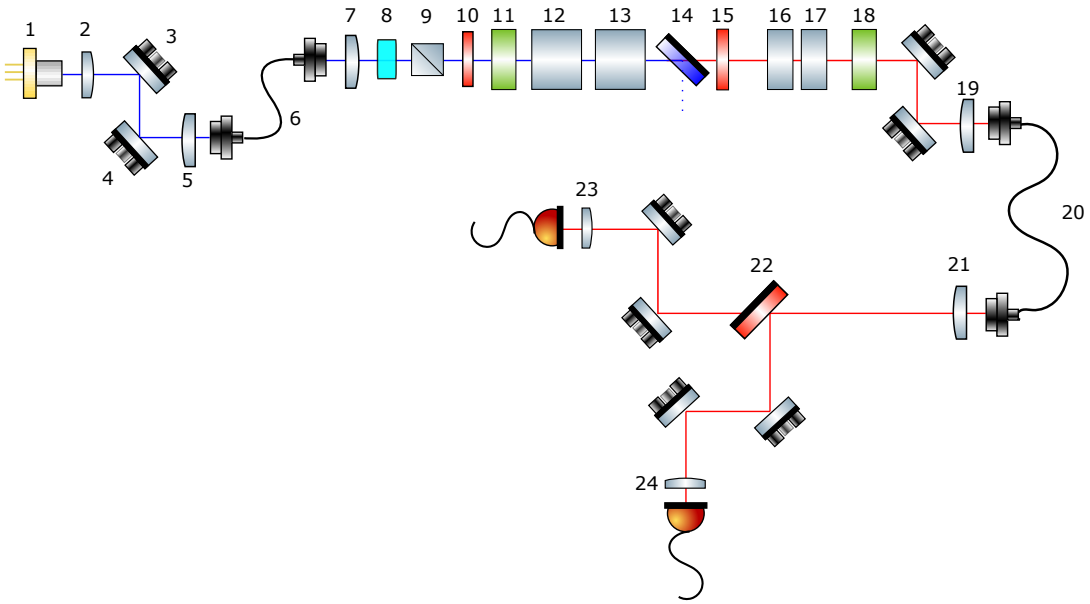


Fig. 2.1: **Schematic showing all the components of the current entangled photon setup**. Single mode blue laser light from fibre (6), polarized at 45° (9&10 passes through the pre-compensator (11). It is focused using an asperic lens (7) between BBO crystal I and II (11 and 12) orientated as explained in text. The pump leaves the optical path (14 and 15) and the downconverted ligth passes through BBO crystal III and IV (16 and 17) and the post compensator (18). It then is coupled into a single mode fibre (20) using a coupling lens (19). The non-degenerate photon pair is split using a dichroic mirror (22) and coupled into multi-mode fibres that go to single photon APDs and counting statistics. Figure through the courtesy of Aitor Villa

There are a couple of reasons why this geometry and type of phasematching is chosen. First, it allows for the source to constructed in a single line, which allows for easier alignment and a mechanically more robust design. It also allows for the components to be miniaturized to a form-factor which fits in the palm of your hand, and more importantly into a cube-sat. Second, the Type-I critical phasematching allows for a collinear set of downconverted photons, that is not dependent on crystal temperature. The temperature of objects in space greatly varies, depending on which side of the earth the sun is. If this would influence the phasematching, it would severly limit the operation of the satelite. Third, it is aimed to achieve the desired performance without the use of actively or passively mechanically stabelized interferometers, which would pose an enormous challenge to remain stable after a launch into orbit.

To obtain a maximally entangled Bell state from this geometry a lot more components are necessary (more on this in 5.1). For this we need to erase the which-crystal information of the photons. We will first identify the sources of which-crystal information in the geometry.

### 2.3.1 Spatial decoherence

One of the degrees of freedom that contains which crystal information is the spatial mode in which the photons are emitted. If the distribution of modes in which the horizontal modes are emitted differ from the vertical ones, the photon pairs will become distinguishable, and the entanglement will be reduced. Due to the walk-off effect of the extraordinary polarized pump, the SPDC photons are emitted in a double ellipse figure, that is elongated over the whole crystal length. To ensure a good spatial overlap, one can use a second pair of birefringent crystals with half the length as the ones in which the downconversion occurs, to spatially overlap the downconverted photons. This will allow for efficient collection from the overlap region. The spatial profile of the light is shown in figure 2.2

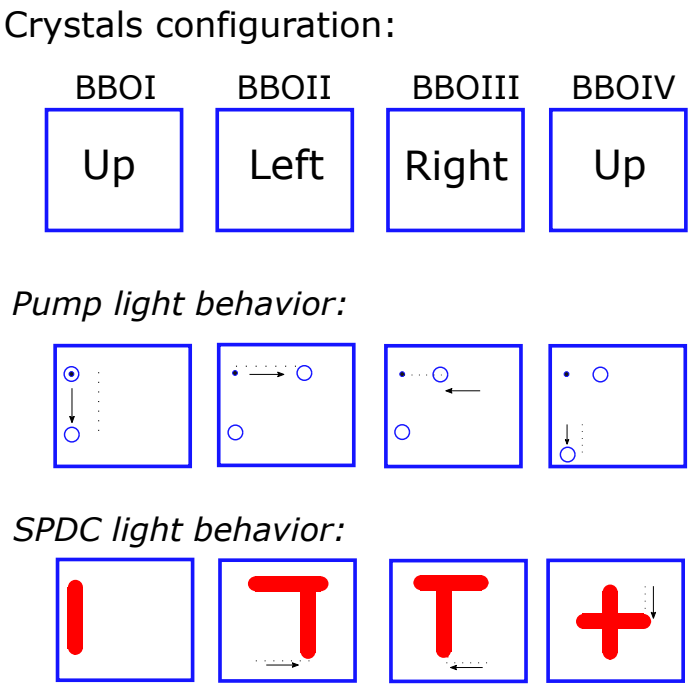


Fig. 2.2: **Overview of the spatial distribution of the light when propagation through the four BBO crystals as shown in fig. 2.1**. Top: Orientation of the optical axis of the BBO crystal when looking from the propagation direction. Middle: Behaviour of the pump light when propagating through the crystals. Note that the pump is filtered out using a dichroic mirror and filter before crystal III and IV. Bottom: the spatial distribution of the downconverted light. The ellipses take the form of the pump waist $w_p$ and the walkoff of the pump in the crystal. The crystals III and IV provide maximal spatial overlap for the centres of these ellipses.

When using optics to efficiently collect these photons, one has to make sure that the spatial modes that are collected are the same for both crystals. In principle, it is possible to collect a multiple of different spatial modes, as long as all these modes are occupied by the same number horizontal and vertical photons, to keep the two indistinguishable. This is however very challenging, and a more effective approach is either using pinholes to limit the spatial modes from which photons are collected, or coupling into a single spatial mode using a single mode fibre. The single mode fibre effectively acts as a pinhole for the downconverted mode. This means however that a lot of photons that emitted in different mode than the TEM00 mode are not collected, reducing the brightness.

### 2.3.2 Temporal decoherence

The spatial dimension is not the only dimension in which the photon pairs might be distinguishable. In the temporal domain the photons also differ slightly, due to the difference in group velocity of the different fields in the crystal. This time delay is schematically shown in fig. 2.3.

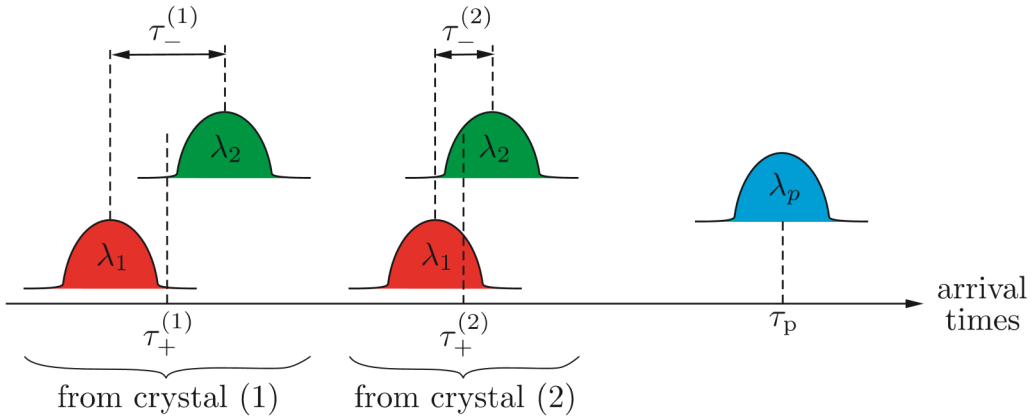


Fig. 2.3: **Schematic representation of the arrival time of the downconverted photons with respect to the pump.**. The arrival time of the signal (idler) photon is shown in red (green). The photon pairs can differ in two timings: the time difference between signal and idler photon ($\tau_-$), or the time difference in arrival time of a downconverted pair with respect to the pump photon ($\tau_+$). Erasing this information is crucial to achieve a highly entangled state. Picture taken from P. Trojek [18]

To compensate for these delays, additional crystals are placed in the setup. If we chose the correct dispersion, birefringence and length of these compensation crystals appropriately, one can influence both $\tau_-$ and $\tau_+$. In practice we use crystals made of $YVO_4$ cut at an angle of $\frac{\pi}{2}$ to compensate both $\tau_-$ and $\tau_+$. The reason for this is the high birefringence of this material, which allows us to compensate with short crystals. More details off the origin of the delays and how to calculate the exact length of the compensator crystals follow in the next chapter.

To calculate the distinguishibility of the photon pairs at different times, we follow the analysis done in this work by R. Rangarajan [19], which calculates the joint two-photon complex amplitude (JTPA) of the wavefunction. We can then write down the density matrix of a quantum state in terms of the arrival times of the signal and idler photons, leading directly to a measure for fidelity with the desired Bell state.

Following their analysis, the unnormalized two photon state can be written as

$$|\Psi\rangle = \int\int f(t_s, t_i)\hat{a}_s^+(t_s)\hat{a}_i^+(t_i)dt_s dt_i|vac\rangle, \tag{2.6}$$

where $f(t_s, t_i)$ is the JTPA, $|vac\rangle$ is the vaccuum state and $\hat{a}_w^+(t_w)$ the creation operator of a $w$ photon at time $t_w$ ($w = s, i$). If we now define a pump with central frequency $\omega_p$ and bandwidth $\sigma_p$, we can define the detunings of the signal and idler photons as $\nu_{s,i} = \omega_{s,i} - \frac{\omega_p}{2}$, and the JTPA can be written as

$$f(t_s, t_i) = \frac{e^{-i\omega_p \frac{t_s+t_i}{2}}}{2\pi} \int\int e^{-i(\nu_s t_s + \nu_i t_i)} e^{-\left(\frac{\nu_s+\nu_i}{\sigma_p}\right)^2} \Theta(\nu_s, \nu_i) d\nu_s d\nu_i \tag{2.7}$$

The first term outside the integral is the phase set by the pump photon, whereas the first term in the integral is the additional phase of the two photon state depending on the time difference of the two photons and their detuning from the pump frequency. This additional phase is scaled by the ratio of the detuning of the down-converted field, with respect to the pump linewidth. The last term, $\Theta(\nu_s, \nu_i)$, is a real function which calculates the probability that a pump photon produces a photon pair at detunings $\nu_s$ and $\nu_i$. This function is given by

$$\Theta(\nu_s, \nu_i) = \left( \frac{\sin(\frac{\Delta k L}{2})}{\frac{\Delta k L}{2}} \right)^2 \tag{2.8}$$

where $L$ is the interaction length of the SPDC fields, and $\Delta k$ is the phase mismatch that can be calculated using 2.2:

$$\Delta k = \|\mathbf{k_p} - \mathbf{k_s} - \mathbf{k_i}\|$$

We can now write the output state of our entangled photon source as, when tracing over the time variable

$$\rho = \frac{1}{2}\big(|HH\rangle\langle HH| + |VV\rangle\langle VV| + v(\Delta t_s, \Delta t_i)|HH\rangle\langle VV| + v^*(\Delta t_s, \Delta t_i)|VV\rangle\langle HH| \tag{2.9}$$

where $v(\Delta t_s, \Delta t_i)$ is defined as the convolution of the JTPA:

$$v(\Delta t_s, \Delta t_i) = \int\int f(t_s, t_i) f^*(t_s + \Delta t_s), t_i + \Delta t_i) dt_s dt_i,$$

and $\Delta t_j = t_{j,H} - t_{j,V}$ the time difference between a signal/idler photon with horizontal/vertical polarization. We now clearly see that when the photons arrive at different times, they arrive with a different phase, which will lead to decoherence in the polarization degree of freedom.

## 2.4 Software

To be able to provide accurate predictions and still have the flexibility of changing many input parameters, a custom ray-tracing module was written in Mathematica. This 3D sequential ray tracing model uses the standard Mathematica language to define the different object geometries and materials used, and can deal with curved spherical surfaces to define lenses.

The downconversion process itself is modeled as a stochastic process, where all the properties of the photons are drawn from distributions defined by the underlying physics. A ray will consist of 3 spatial coordinates $r = (x, y, z)$ where $z$ is the propagation direction, and two angular coordinates $(\alpha, \beta)$, where $\alpha, \beta$ is the direction cosine in the $x, y$ direction. Each ray has a polarization, where vertical corresponds to the $x$ direction and a wavelength $\lambda$. See tab. 2.1 for the details, and 5.2 for some visual examples.

Table 2.1: **Table showing methods for initial starting parameters for the down-converted photon pair.** The initial position of the photon pair is a single coordinate $r$, where the $x$ and $y$ coordinates are drawn from a Gaussian intensity profile of the pump, and takes into account the walkoff of the pump. The direction and wavelength of the signal are drawn from the normalized phasematching function, and the idler parameters are chosen accordingly. This is done for both crystals where the downconversion process happens.

| Ray | $r_{start}$ | $(\alpha, \beta)$ | Polarization | Wavelength |
|---|---|---|---|---|
| Signal | Random from pump intensity | From eq. 2.8 | H or V | From eq. 2.8 |
| Idler | Same as signal | -$(\alpha, \beta)$ from Signal | Same as signal | From eq. 2.1 |

The polarization and wavelength dependant refractive index of the media is calculated for each individual photon that enters the object. The photon travels from surface to surface, until it hits the last surface. By applying different filtering steps on the set of rays that reach the end of the setup we can simulate the coupling of the rays into a single mode fibre. This is done by only accepting rays that hit the virtual core of the fibre at an angle that is smaller than the numerical aperture of the fibre. A small schematic from the result of a simulation is shown in fig. 2.4. The raw data of trajectory and effective optical path is saved in a matrix format.

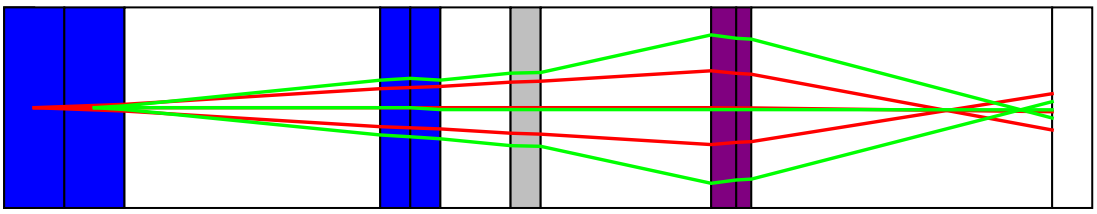

Fig. 2.4: **Sideview (yz – plane) of the ray tracing of 3 horizontal (vertical) rays in red (green) through 3 different types of objects (not to scale)**. The blue objects are of material BBO, grey is $YVO_4$ and purple is glass achromatic lens contaning two pieces of glass (curvature not showing). The refraction not following Snell's law is due to the polarization of the ray being extraordinary in that medium. There is no walkoff in the grey crystal because of the specific cut angle.

This approach lends its validity from the fact that the downconversion process is not a coherent process in time, meaning that the overall phase for the downconversion field is not well defined, and varies from downcoversion event to event. The only correlations are in the phase difference between signal and idler photon, that is defined by the pump photon. Therefor the process can be treated like individual pairs of photons, and are incoherently coupled into a single mode fibre.

In a later stage of the project the ray tracing software OpticStudio 16.5 [20] was used, which is the industry standard when looking at illumination and light profiles for different geometries and materials. This provided an enormous speed-up when trying to trace a big amount of rays, but it severly limited the access of raw data of the simulation. Additionally, Mathematica was still used to define the initial set of rays that are used in the simulation run in OpticStudio.

The tools described in this chapter give us a powerful method to investigate the spatial and temporal behaviour of the downconverted photon pairs in our collineair geometry. This allows us to determine the appropriate methods to compensate these sources of decoherence, and describe the limits for which our compensation techniques no longer work.

# Chapter 3

# Results and Discussion

This chapter will be divided into two parts. The first part will cover the temporal decoherence due to the difference in signal and idler arrival time ( $\tau_-$, see fig. 2.3). In this part we will also discuss the difference in using an aspheric or achromatic lens to collect the SPDC light, the effects of filtering the signal photons and using shorter crystals. The second part will consists of the analysis of the temporal decoherence due to the difference in arrival time of the horizontal and vertical photons ($\tau_+$ from fig. 2.3). This will consists of an analysis of the effect of decreasing the pump coherence time and uncertainties in the crystal lenght.

## 3.1 Decoherence due to $\tau$.

The amount of which-crystal information in the parameter $\tau_-$ depends on the coherence time of the downconverted photons. If $\tau_-$ exceeds the coherence time of the photons, there is a lot of information in this parameter, and the photons will be completely distinguishable. On the other hand, if $\tau_-$ is much smaller than the coherence time, there is no measurement that extracts information from which crystal the photon came in this parameter. One approach to prevent decoherence in this paramter is thus to increase the coherence time of the photons, which means spectrally filtering the light fields. This however will greatly reduce the amount of photon pairs detected, because the SPDC process is a broadband process, and the linewidth of the signal and idler field is usually on the order of 30nm, depending on the phasematching conditions and crystal length. For a high brightness source, it is more desirable to use compensation crystals to bring $\tau_-$ well below the temporal coherence of the SPDC light.

### 3.1.1 Origin.

The origin of the which crystal information for the time difference $\tau-$ is due to the co linear geometry of the setup. The signal/idler pair that originates in crystal I will travel through crystal II, III and IV, where a signal/idler pair from crystal II will only pass through III and IV. During that passing through the crystal the photons are extra-ordinary polarized, and the signal and idler photon have a slightly different refractive index due to the dispersion of the material. The dispersion in the crystal where the photons get downconverted will be equal for H and V polarizations, so

this will not contribute to time difference $\tau_-$. The same argument can be made for the crystals III and IV.

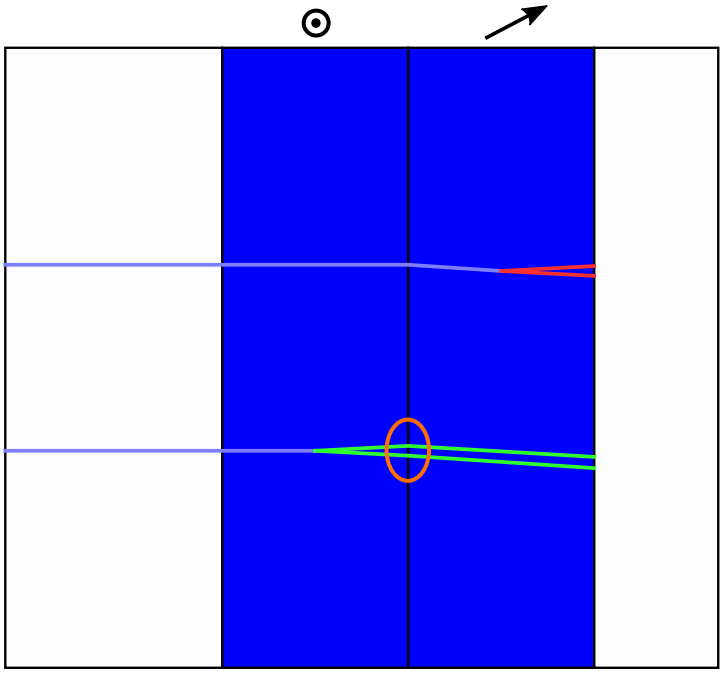

Fig. 3.1: **Top view of ray tracing of two signal/idler pairs through crystals I and II, showing the difference in optical path length.** The photons downconverted in the first(second) crystal are shown in green(red), originating from a pump photon (blue), offset for clarity. The green photons experience walkoff in the same direction of the pump, due to the orientation of the optical axis of the crystals, shown at the top. The exact value of the time delay can be calculated by using the angle of incidence at the interface between the crystals, clarified by the orange circle, and the exact crystal length. Colour does not indicate wavelength.

A schematic showing the different paths of the two photon pairs is shown in fig. 3.1. Shown from the top is the difference in optical path length of the photon pairs originating from the centre of crystal I and II. Both the photon pairs are shown with a small opening angle (exaggerated for clarity). This opening angle arises naturally from the phasematching conditions (eg. 2.2), and even though the crystals are machined such that the maximum intensity is at 0°, a significant number of photons are emitted at angles of $\approx 0.7°$. This opening angle is also the angle of incidence of the downconverted photons on the interface between crystal I and II, as shown in fig. 3.1. This leads to a time difference $\tau_-$ that is dependent in the emission angle of the downconverted photons.

### 3.1.2 Compensation

To correct for the average time difference $\tau_-$, at opening angle 0°, we place a positive birefringent crystal (material $YVO_4$, cut angle $\frac{\pi}{2}$) in the path of the downconverted photons. In this crystal, the photon pairs originating from crystal II are now extraordinary polarized, and due to the dispersion the signal photon will be delayed more with respect to the idler than for the photon pair from crystal I, which are ordinary polarized. After propagating through the whole length of this crystal, the value of the parameter $\tau_-$ is greatly reduced, well below the coherence time of the downconverted field. This is shown in fig. 3.2

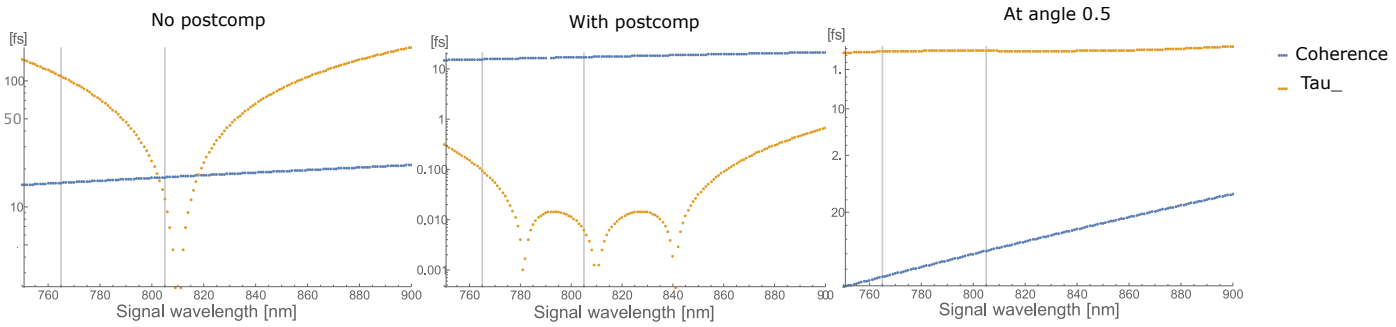


Fig. 3.2: **Effect of post compensation on the parameter $\tau_-$.** Left: without any compensation, only the degenerate photons have a $\tau_-$ smaller than the coherence time of the SPDC field. Middle: with an appropriate compensator crystal of $YVO_4$ the photons are compensated over a broad wavelength. The sharp dips are the wavelengths for which the source is designed. Note the change in axes. Right: Same setup as middle, but now the comparison is done for a signal/idler pair at an opening angle of 0.5°. This leads to imperfect compensation, and in result a lower fidelity Bell state. Parameters for this simulation: BBOI & II $L = 6$ mm, $\theta_c = 28.799°$, BBOIII & IV $L = 3$ mm, $\theta_c = 28.799$ and compensator $YVO_4$, $L = 3.121$ mm, $\theta_c = 90°$. Pump, signal and idler wavelenghts are 405 nm,785 nm and 832 nm respectively, with line-width of SPDC $\Delta\lambda = 40$ nm.

This method of temporal compensation however is sensitive in the opening angle of the signal/idler pair. Due to the type I phasematching used, photons with a bigger opening angle will be badly compensated. This is shown in the right of 3.2. This has implications on the collection of the downconverted photons. When using focussing optics to collect efficiently from the crystals, photon pairs emitted at bigger opening angles are collected than when using a collimated collection. This leads to degradation of the produced state fidelity with the maximally entangled Bell state.

### 3.1.3 Measurements

This was observed in the lab when two different lenses were used in the collection of the entangled photon. The first lens is an achromatic doublet built by Thorlabs (AC-080-16 ML), the second lens is an aspheric lens from Thorlabs (A375-B ML). The effect was persistant, even when changing the FWHM of the focus of the Gaussian collection beam, using different focal length achromats. When collecting from 6mm crystals with an achromatic lens, the measured visibility would never reach above $\approx 80\%$, unless a spectral filter $\Delta\lambda = 13$nm was used. With an aspheric lens however, high visibility (+95%) was obtained wihtout the use of a filter. Using the software

OpticStudio 16.5, we could simulate the difference in angular distribution of the collected photons, see App. 5.3. This angular distribution could then be converted to the parameter $\tau_-$ and compared to the coherence time of the SPDC field with and without a filter. This is shown in figure 3.3.

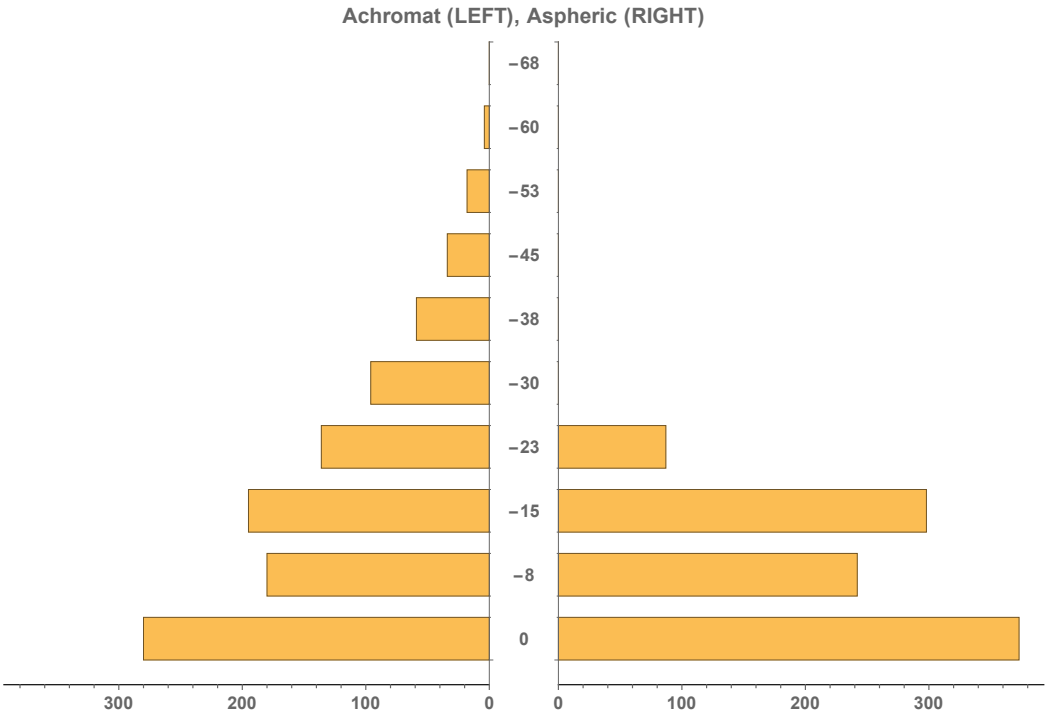


Fig. 3.3: **Histogram of difference in temporal compensation of signal/idler pairs with 2 types of lenses.** This double histogram shows the distribution of the $\tau_-$ parameter when collection with an achromatic doublet (left) or aspheric lens (right). X-axis shows occurrance, y-axis shows the parameter $\tau_-$ for the respective bin in femto-seconds. Using 2.9 the visibility of the measured interference pattern can be calculated, showing $0.78 \pm 0.04$ and $0.92 \pm 0.04$ for the achromat and asphere respectively. This agrees with the $0.80 \pm 0.02$ and $0.98 \pm 0.01$ measured in the experiment. $\tau_-$ times are calculated with the same parameters as fig. 3.2

This phenomenon can explain how the unfiltered photons collected with the achromat do not produce a state with high entanglement without the need of a spectral filter to increase the coherence time. Additionally, from the phasematching conditions we can derive that the photons that get generated with an opening angle, deviate from the central design wavelengths, so the spectral filter acts as an angular filter as well.

This problem of decoherence due to opening angle can also be solved by using shorter BBO crystals to build the entangled source. This will reduce the spread in $\tau_-$ because of the short distance over which the signal/idler pair experiences walk-off. The same compensation of the mean value can be achieved by using a smaller $YVO_4$ crystal. This has been experimentally verified, the results are summarized in tab. 3.1

Table 3.1: **Table showing experimental results when collecting from different lengths crystals with an achromatic doublet.** The decoherence due to the opening angle is reduced when using shorter crystal, resulting in a higher visibility in an interference measurement. The usage of a filter, restricting the signal line-width to 13nm, increases the measured visibility for both the setups. Due to the shorter crystals, the average value of $\tau_-$ is reduced by a factor of 3, so that with the appropriate filtering high visibility is possible without any compensation crystals, as mentioned in the beginning of the chapter. Collection for all setups done with achromatic doublet (AC-080-16 B ML).

| BBOI & II L | Post-comp L | $\Delta\lambda$ signal | Visibility | Brightness |
|---|---|---|---|---|
| 6 mm | 3.12 mm | $\approx 40$ nm | $0.80 \pm 0.02$ | 17.8k counts/s/mw |
| 6 mm | 3.12 mm | $\approx 13$ nm | $0.93 \pm 0.02$ | 7.3k counts/s/mw |
| 2 mm | 1.04 mm | $\approx 50$ nm | $0.98 \pm 0.01$ | 17.8k counts/s/mw |
| 2 mm | 1.04 mm | $\approx 13$ nm | +0.98 | - |
| 2 mm | 0 mm | $\approx 13$ nm | $0.92 \pm 0.02$ | 7.2k counts/s/mw |

More recent experiments using fibres with different numerical apertures show that using a low NA fibre will also reduce the number of photon pairs with a high opening angle. These experiments are however ongoing.

## 3.2 Decoherence due to $\tau_+$

The second temporal parameter that can contain which-crystal is the difference between the arrival time of the downconverted two photon state with respect to the pump photon for the two polarization states, as shown in fig. 2.3. Just like the parameter $\tau_-$, if this value exceeds the coherence time of the overall wavepackets, it contains a lot of information about which crystal the downconverted state came from. If the arrival time of a pump photon has a big uncertainty, which is the case for a narrow linewidth/high coherence time pump laser, the relatively small difference between signal/idler pairs coming from crystal I and II will not give away any information.

Recent experiments have shown that with the current setup we are not able to achieve sufficiently high visibility with a laser diode other than the Ondax VHG diode, see tab. 3.2. This laserdiode is very narrow and thus allows us to neglect the compensation of the $\tau_+$ parameter. The mediocre power output and mode hopping due to temperature fluctuations make this laser diode not ideal for operation in a space-environment, and other options that are more stable and have higher power are considered, see 3.2.

Table 3.2: **Table showing blue laser diodes used that have been used in past experiments.** The linewidth of the blue laser diodes are either $\approx 1$ nm, or very narrow, with little availability in between. The last laser from Sanyo has not been tried yet in an experiment. So far only the laser from Ondax has produced photon pairs that have high fidelity with the Bell state. This laser however lacks the optical power to achieve a bright enough source for our applications.

| Vendor | Model | Central | $\Delta\lambda$ | Nom. Power | High Visibility |
|---|---|---|---|---|---|
| Nichia | NDV4316 | $405 \pm 5$ nm | $\approx$ 1nm | 140mw | No |
| Sanyo | DL-LS5017 | $405 \pm 10$ nm | $\approx$ 0.8nm | 65 mW | No |
| Thorlabs | L405P150 | $405 \pm 5$ nm | 2.3nm | 150 mW | No |
| Ondax | X6105 | $405 \pm 1$ nm | 160Mhz | 40 mW | Yes |
| Sanyo | CL-714-101 | $405 \pm 10$ nm | $< 0.15$nm | 100 mW | N.A. |

### 3.2.1 Origin

The origin of the which crystal information for the time difference $\tau_+$ is again the colinear geometry of the setup. The average group velocity of a downconverted photon pair through the BBO crystal is slower than the group velocity of the pump photon. This is shown in fig. 3.4.

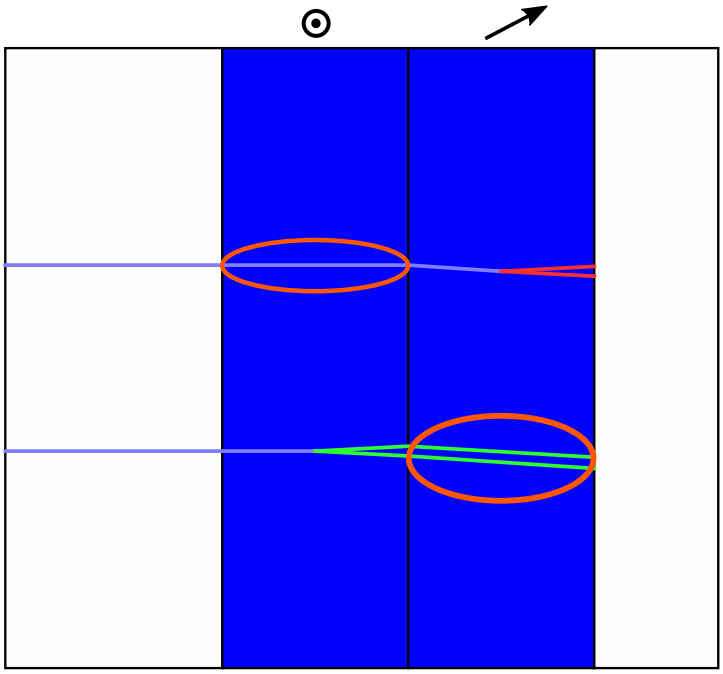

Fig. 3.4: **Top view of ray tracing of two signal/idler pairs through crystals I and II, showing the difference in optical path length.** Schematic identical to 3.1, showing the origin of the difference in arrival between the two photon state originating in the first and second crystal. The optical path of the pump photon that gets downconverted in the second crystal (upper orange circle) is shorter than the optical path of the downconverted photons that originate from the first crystal (lower orange circle). Colour does not indicate wavelength.

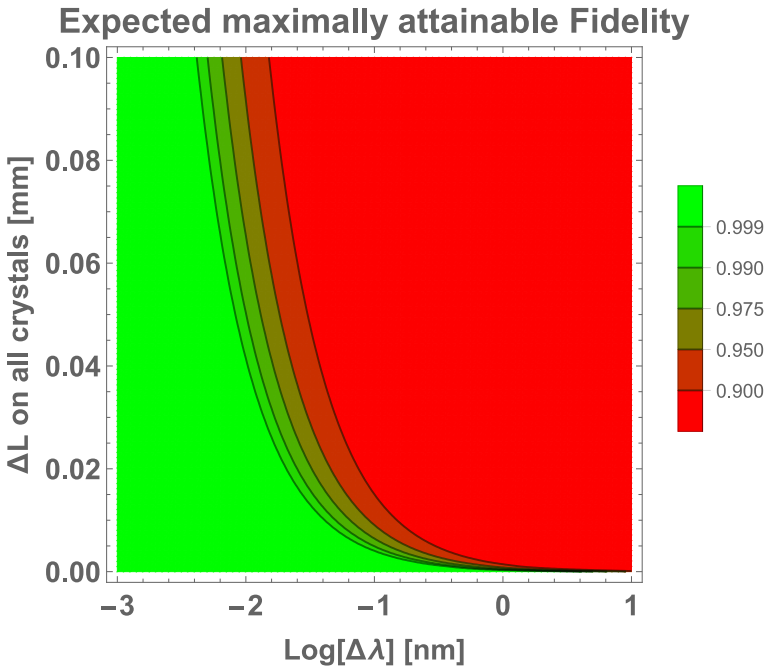


Fig. 3.5: **Contour plot showing the estimated maximum achievable visibility at differed machining accuracies and pump coherence times.** Red regions indicate a visbility unacceptable for our experiments. Green areas indicate that the parameter $\tau_+$ will not be the limiting factor in the setup. This graph shows that the current geometry of the entangled source can not be successful for broad line-width laser diodes.

### 3.2.2 Compensation

To compensate for this effect, a birefringent retarder (material $YVO_4$, crystal cut at 90°) is placed in the path of the pump beam. This will provide a delay for the horizontally polarized photons, that will get downconverted in crystal II. If there is a post compensation $YVO_4$ crystal used in the setup, the delay of the horizontal with respect of the vertical photons will also need to be taken into consideration when calculating the length of the precompensation crystal.

This method to compensate for the time difference is limited by the accuracy with which the crystals are machined, which is currently ±0.1mm. If the crystals length can not be machined with adequate accuracy, the temporal compensation cannot be accurate enough to produce a state with high fidelity with the Bell state, depending on pump coherence. To replicate the 'blind' ordering of the crystals from a manufacturer, we can draw the crystal length L from a normal distribution with mean the desired length and standard deviation the machining tolerance. We can then build the setup and calculate the time delay for that specific set of crystals. By repeating this many times we can define an expected value for this procedure. This expected value of $\tau_+$ is what we are limited by due to the manufacturing process.

The crystals could be measured accurately upon arrival and cherry picked to form the best possible configuration, but that would require buying many more crystals then we need, to increase the chances of finding a good set. This is not an option for producing many units with the same specifications. Figure 3.5 shows the expected attainable visibility, given all other which-crystal information is erased, when using crystals machined at a specific tolerance.

### 3.2.3 Impact

Figure 3.5 shows that with the current crystal tolerance of $\pm 0.1$ mm, a laser diode with a line-width $< 0.005$ nm is needed to ensure that the visibility is not limited by the pump coherence. When ordering better machined crystals, with tolerances $\pm 0.01$ mm, the line-width of the laserdiode can be relaxed to 0.15nm. This realization has led to the ordering of new sets of crystals, and the search for high power laser diodes with appropriate line-width has intensified. The search for another, more sensitive compensation method has been started, where one of the options is to use a double wedge shape of $YVO_4$. The calculations of the sensitivity of compensation and effective range of this method are still under investigations. If this method is proven succesfull it would be of great value in compensating the $\tau_+$ delay of the SPDC photons.

# Chapter 4

# Conclusion and Outlook

In this work, significant progress in understanding the limiting factors of our compact entangled photon source has been made. Building on previous work, a ray tracing tool to describe the propagation and collection of single photon pairs has been written. It was used to provide insight into two problems currently facing the construction of a compact, high-brightness entangled photon source for novel experiments and applications in space.

First, the importance of recognizing effect of the opening angle on the temporal compensation between signal and idler photons, has led to the explanation of a experimental struggle in achieving high visibility. Depending on the coherence of the down-converted photons, the solid collection angle at which you should collect from the crystals must be carefully chosen. The ray-tracing software will predict for which angles the compensation is still successful. Furthermore, achromatic doublets and aspherical lenses have shown a difference in collection pattern, which explained their difference in performance quantitatively. The possiblities to test the performance of other components, such as pinholes and fibres will be a valuable continuation of this work. The ray-tracing software will also aid in the design of other elements that might be added to the setup, such as collimation lenses to increase coupling efficiency, and pinholes to take over the role of single mode fibres.

Second, the reason why the construction of an entangled source with a broad line-width laser has remained unsuccessful so far has been discovered. The choice to use more powerful but less coherent lasers is to increase the absolute brightness of the source. The current machining tolerances of the length of the used crystals turned out to be unable to compensate the arrival time of the horizontally and vertically polarized two-photon states to below the limit set by the laser diode. To increase entanglement visibility of the source, more coherent laser diodes, as well as better machined crystals are ordered.

The ray-tracing module can work with any number of rectangular shapes of $YVO_4$ and BBO, as well as spherical lenses made from different materials. This allows the user to be able to quickly adjust the parameters of any of the crystal, as well as adding collimation and collection lenses in any place. Additional steps to include Potassium Titanium Oxide Phosphate (KTP) into the simulations have already been taken, to perform similar calculations. The addition of OpticStudio 16.5 has been used to more rigorously calculate the performance of different lenses. In the future, the optimization function of this software might be useful in calculating the best positions of certain lenses and pinholes in our geometry, reducing the

amount of options that have to be tried by hand in the lab.

As a recommendation to improve the performance of the photon source, a couple of ideas come to mind. First, the lens/fibre configuration in the collection path should be optimized to couple in the photons that are emitted at a small opening angle. Even though the increased brightness of collecting more photons seems tempting, these will decohere the state and will not improve the performance. Second, the usage of pinholes to restrict the spatial mode of the SPDC instead of a single mode fibre (SMF) might increase the overall brightness of the source. The coupling of divergent incoherent light into a small fibre remains a challenging task, and using a different method to ensure a single spatial mode might prove successful. As mentioned before, the usage of special SMF is still an ongoing work of research.

In conclusion, the usage of ray-tracing to describe the propagation of the SPDC field in a co-linear, type-I phasematched entangled photon source has lead to a better understanding of the sources of decoherence in our setup. It will also allow to further help the progress of the team in building a compact, high brightness and fidelity entangled photon source for novel applications, both in space and on the ground.

# Chapter 5

# Appendices

## 5.1 Word on entanglement via SPDC processes.

The SPDC process produces photons highly correlated in many degrees of freedom. Not only are the polarizations of the signal and idler correlated because of the phasematching, due to energy conservation they are also correlated in wavelength. Other degrees of freedom like orbital angular moment of higher order spatial modes are also correlated, due to the conservation laws nature abides. In general however this does not mean that the photons are *entangled*, which requires more than just correlations.

To go from a correlated to an entangled photon pair one must make sure that the photons are indistinguishable at the time that they are measured, except for the one property where they are entangled in. In our case, in which we produce photons entangled in the polarization degree of freedom, this means that the photons produced with horizontal polarization have to be indistinguishable from the ones produced with vertical polarization in all other degrees of freedom.

This does not mean that all the other properties of the photons need to be fixed to one and the same value. This would make the generation of entanglement with this method impossible, because of the random nature of the SPDC process. It means that we need to reduce the difference between that the horizontal and vertical photons might have in a certain degree of freedom, below the intrinsic randomness of the individual downconversion processes.

So for all the parameters for which there might be information about form which crystal the photons came, one has to find the corresponding coherence time or *intrinsic* randomness, to find out if the information is buried under a layer of randomness by nature, or if they are easily told apart.

## 5.2 Spatial and angular origin of the SPDC light

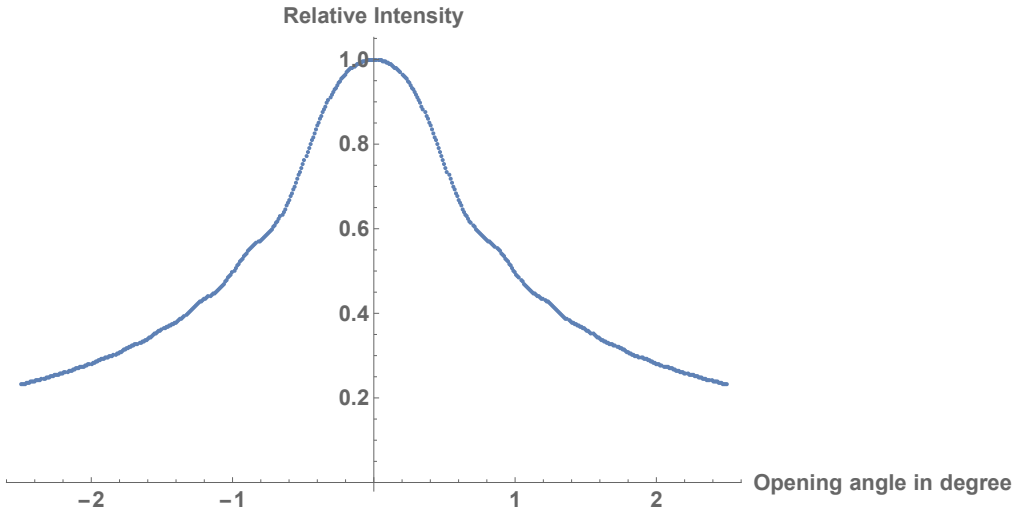


Fig. 5.1: **Figure showing the opening angle distribution of the down-conversion photon pairs in two BBO crystals of 6mm.** Using the phase matching conditions, see 2.1, the relative intensity of the SPDC photons with respect to the opening angle can be calculated. This graph shows the result of a 6 mm BBO crystal with $\theta_c = 28.7991°$ pumped at 405 nm. Even at higher opening angles there is still a significant amount of emitted SPDC light.

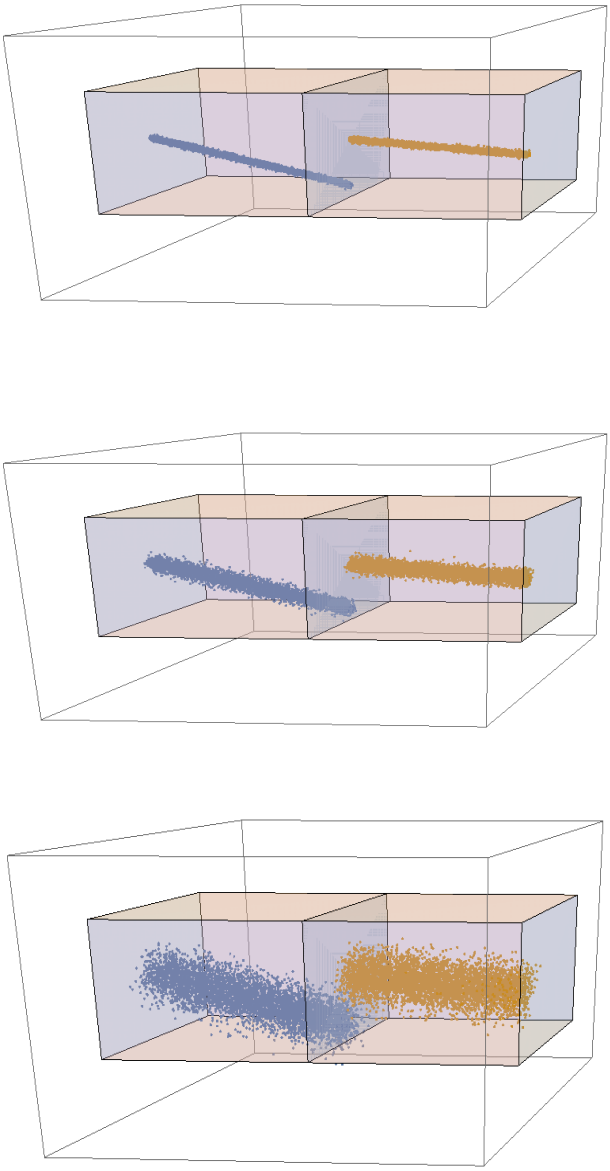

Fig. 5.2: **Figure showing the spatial distributions of the down-conversion points in two BBO crystals of 6mm.** Using the underlying physical conditions such as phase-matching and energy conservation, see sec. 2.1 and 2.4, the intial starting points and opening angles for the signal/idler pairs are calculated. Showing the simulations for a pump waist of $50, 100$, and $200$ $\mu$ respectively from top to bottom. Crystal width in plot is 1mm (real crystals are 6 mm), crystal length is 6 mm.

.

## 5.3 Figures of Zemax simulations

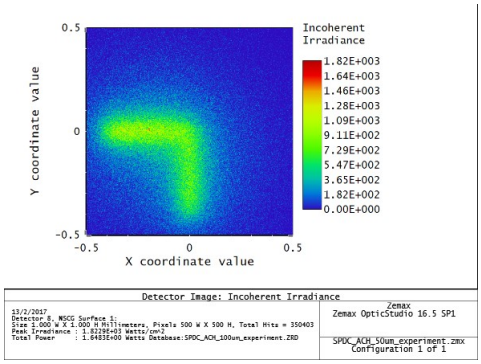


(a) Complete spatial distribution of SPDC light.

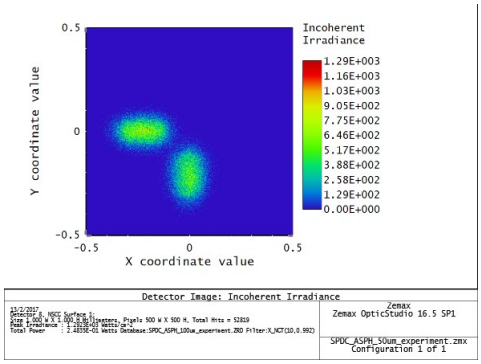


(b) Spatial distribution of SPDC light collected with ashperical lens (A375-B-ML)

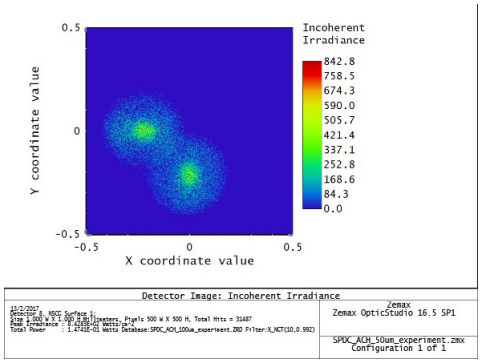


(c) Spatial distribution of SPDC light collected with Achromatic doublet lens (AC-080-16-B-ML)

Fig. 5.3: **Figure showing the difference in collection patter between aspheric and achromatic lenses.** This figure shows the intensity of the SPDC light coupled into a SMF ( 5 $\mu$m core diameter, NA = 0.12) at the position after BBO II (fig. **??**). The lens and fibre are placed at a (local) optimum for the brightness of the source. This allows us to see from which part the lens is collecting. Left: the full intensity of the SPDC light, clearly showing the double elliptical pattern (not yet spatially compensated). Middle: collected part with an aspheric lens. It shows that the collection happens for a large distance along the optical axis, coming from the middle of the crystal, with relatively small opening angle (reduced size of ellipse width). Right: collected part with an achromatic lens, showing a collection that is more narrow in space along the optical axis, but broader in acceptance angle (round shape of the intensity profile). A histogram of the opening angles can be made, and used in a analysis of final state fidelity, see sec. 3.1.3

.

## 5.4 Building crystals with ΔL tolerances.

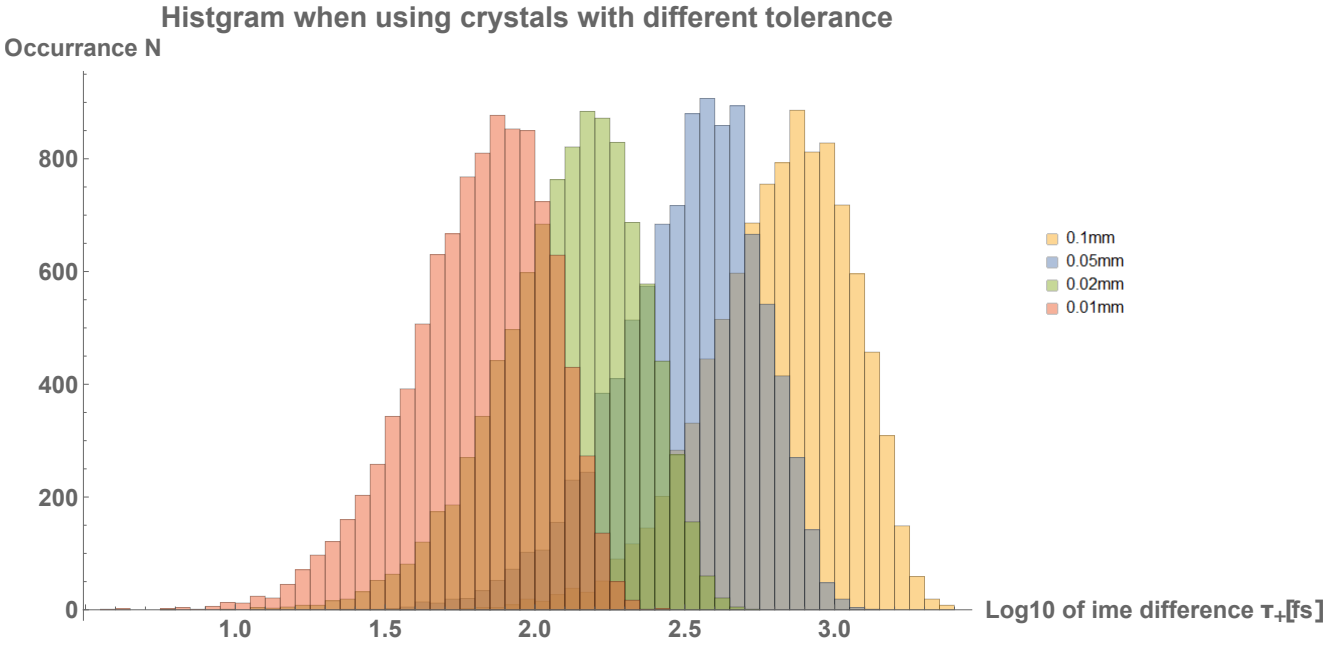


Fig. 5.4: **Histogram of $\tau_+$ of 6mm BBOI & BBOII length entangled photon source with pre and postcomp, all crystal having varying tolerances.** Drawing all the crystals used in a setup from a distribution with mean the design length, and standard deviation the factory machining tolerance. Reducing the tolerance by and order of magnitude, improves the average error in compensation with almost 1.5 orders of magnitude

.

# Bibliography


[1] A. Lamas-Linares, J. C. Howell, and D. Bouwmeester. Stimulated emission of polarization-entangled photons. *Nature*, 412(6850):887–890, Aug 2001. ISSN 0028-0836. doi: 10.1038/35091014.

[2] Paul G. Kwiat, Edo Waks, Andrew G. White, Ian Appelbaum, and Philippe H. Eberhard. Ultrabright source of polarization-entangled photons. *Phys. Rev. A*, 60:R773–R776, Aug 1999. doi: 10.1103/PhysRevA.60.R773. URL `http://link.aps.org/doi/10.1103/PhysRevA.60.R773`.

[3] Paul G. Kwiat, Klaus Mattle, Harald Weinfurter, Anton Zeilinger, Alexander V. Sergienko, and Yanhua Shih. New high-intensity source of polarization-entangled photon pairs. *Phys. Rev. Lett.*, 75:4337–4341, Dec 1995. doi: 10.1103/PhysRevLett.75.4337. URL `http://link.aps.org/doi/10.1103/PhysRevLett.75.4337`.

[4] Andreas Muller, Wei Fang, John Lawall, and Glenn S. Solomon. Creating polarization-entangled photon pairs from a semiconductor quantum dot using the optical stark effect. *Phys. Rev. Lett.*, 103:217402, Nov 2009. doi: 10.1103/PhysRevLett.103.217402. URL `http://link.aps.org/doi/10.1103/PhysRevLett.103.217402`.

[5] Lynden K. Shalm, Evan Meyer-Scott, Bradley G. Christensen, Peter Bierhorst, Michael A. Wayne, Martin J. Stevens, Thomas Gerrits, Scott Glancy, Deny R. Hamel, Michael S. Allman, Kevin J. Coakley, Shellee D. Dyer, Carson Hodge, Adriana E. Lita, Varun B. Verma, Camilla Lambrocco, Edward Tortorici, Alan L. Migdall, Yanbao Zhang, Daniel R. Kumor, William H. Farr, Francesco Marsili, Matthew D. Shaw, Jeffrey A. Stern, Carlos Abellán, Waldimar Amaya, Valerio Pruneri, Thomas Jennewein, Morgan W. Mitchell, Paul G. Kwiat, Joshua C. Bienfang, Richard P. Mirin, Emanuel Knill, and Sae Woo Nam. Strong loophole-free test of local realism. *Phys. Rev. Lett.*, 115:250402, Dec 2015. doi: 10.1103/PhysRevLett.115.250402. URL `http://link.aps.org/doi/10.1103/PhysRevLett.115.250402`.

[6] Johannes Handsteiner, Andrew S. Friedman, Dominik Rauch, Jason Gallicchio, Bo Liu, Hannes Hosp, Johannes Kofler, David Bricher, Matthias Fink, Calvin Leung, Anthony Mark, Hien T. Nguyen, Isabella Sanders, Fabian Steinlechner, Rupert Ursin, Sören Wengerowsky, Alan H. Guth, David I. Kaiser, Thomas Scheidl, and Anton Zeilinger. Cosmic bell test: Measurement settings from milky way stars. *Phys. Rev. Lett.*, 118:060401, Feb 2017. doi: 10.1103/PhysRevLett.118.060401. URL `http://link.aps.org/doi/10.1103/PhysRevLett.118.060401`.

[7] Matthias Steiner, Victor Leong, Mathias Alexander Seidler, Alessandro Cere, and Christian Kurtsiefer. Time-resolved scattering of a single photon by a single atom. In *Conference on Lasers and Electro-Optics*, page FM3C.8. Optical Society of America, 2016. doi: 10.1364/CLEO_QELS.2016.FM3C.8. URL `http://www.osapublishing.org/abstract.cfm?URI=CLEO_QELS-2016-FM3C.8`.

[8] Zong Sheng Tang, Kadir Durak, and Alexander Ling. Fault-tolerant and finite-error localization for point emitters within the diffraction limit. *Opt. Express*, 24(19):22004–22012, Sep 2016. doi: 10.1364/OE.24.022004. URL `http://www.opticsexpress.org/abstract.cfm?URI=oe-24-19-22004`.

[9] Artur K Ekert. Quantum cryptography based on bell's theorem. *Physical review letters*, 67(6):661, 1991.

[10] Ivan Marcikic, Antía Lamas-Linares, and Christian Kurtsiefer. Free-space quantum key distribution with entangled photons. *Applied Physics Letters*, 89(10): 101122, 2006.

[11] Hiroki Takesue and Kyo Inoue. Generation of polarization-entangled photon pairs and violation of bell's inequality using spontaneous four-wave mixing in a fiber loop. *Phys. Rev. A*, 70:031802, Sep 2004. doi: 10.1103/PhysRevA.70.031802. URL `http://link.aps.org/doi/10.1103/PhysRevA.70.031802`.

[12] Andreas Muller, Wei Fang, John Lawall, and Glenn S. Solomon. Creating polarization-entangled photon pairs from a semiconductor quantum dot using the optical stark effect. *Phys. Rev. Lett.*, 103:217402, Nov 2009. doi: 10.1103/PhysRevLett.103.217402. URL `http://link.aps.org/doi/10.1103/PhysRevLett.103.217402`.

[13] Fabian Steinlechner, Pavel Trojek, Marc Jofre, Henning Weier, Daniel Perez, Thomas Jennewein, Rupert Ursin, John Rarity, Morgan W Mitchell, Juan P Torres, et al. A high-brightness source of polarization-entangled photons optimized for applications in free space. *Optics express*, 20(9):9640–9649, 2012.

[14] Kadir Durak, Aitor Villar, Brigitta Septriani, Zhongkan Tang, Rakhitha Chandrasekara, Robert Bedington, and Alexander Ling. The next iteration of the small photon entangling quantum system (speqs-2.0), 2016. URL `http://dx.doi.org/10.1117/12.2212078`.

[15] Robert Bedington, Edward Truong-Cao, YC Tan, Cliff Cheng, Kadir Durak, J Grieve, Jesper Larsen, Daniel Oi, and Alexander Ling. Deploying quantum light sources on nanosatellites ii: lessons and perspectives on cubesat spacecraft. In *SPIE Security+ Defence*, pages 964811–964811. International Society for Optics and Photonics, 2015.

[16] Zhongkan Tang, Rakhitha Chandrasekara, Yue Chuan Tan, Cliff Cheng, Kadir Durak, and Alexander Ling. The photon pair source that survived a rocket explosion. *Scientific reports*, 6, 2016.

[17] Tang Zhongkan, Rakhitha Chandrasekara, Tan Yue Chuan, Cliff Cheng, Luo Sha, Goh Cher Hiang, Daniel Oi, and Alexander Ling. Generation and analysis

of correlated pairs of photons on board a nanosatellite. In *CLEO: Science and Innovations*, pages JTh4A–3. Optical Society of America, 2016.

[18] Pavel Trojek. *Efficient generation of photonic entanglement and multiparty quantum communication*. PhD thesis, lmu, 2007.

[19] Radhika Rangarajan, Michael Goggin, and Paul Kwiat. Optimizing type-i polarization-entangled photons. *Opt. Express*, 17(21):18920–18933, Oct 2009. doi: 10.1364/OE.17.018920. URL `http://www.opticsexpress.org/abstract.cfm?URI=oe-17-21-18920`.

[20] Zemax. Opticstudio 16.5.